

Structure sensitivity reaction of chloroform hydrodechlorination to light olefins using Pd catalysts supported on carbon nanotubes and carbon nanofibers

Sichen Liu^a, Carlos Fernandez-Ruiz^a, Ana Iglesias-Juez^b, Maria Martin-Martinez^c, Jorge Bedia^a, Carlo Marini^d, Giovanni Agostini^d, Juan José Rodríguez^a, Luisa María Gómez-Sainero^{a,*}

^a Departamento de Ingeniería Química, Facultad de Ciencias, Universidad Autónoma de Madrid, C/Francisco Tomás y Valiente, 7. Campus de Cantoblanco, 28049 Madrid, Spain

^b Instituto de Catálisis y Petroleoquímica, CSIC, C/Marie-Curie 2, 28049 Madrid, Spain

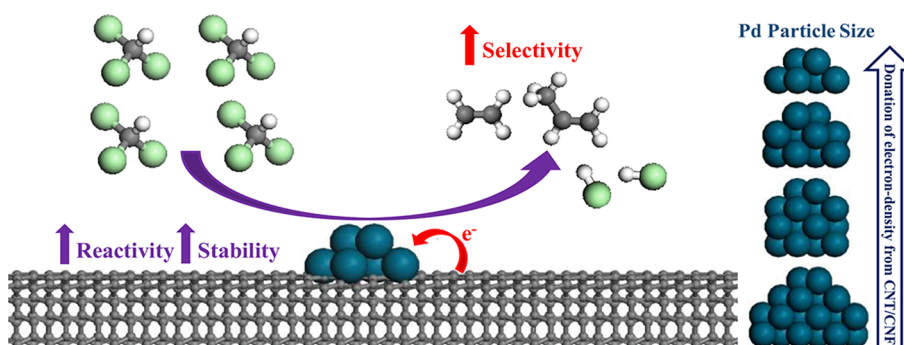
^c Grupo CyPS, Dto. Ingeniería Química y de Materiales, Universidad Complutense de Madrid, Avda. Complutense s/n, 28040 Madrid, Spain

^d ALBA Synchrotron, Carrer de la Llum No. 2-26, Cerdanyola del Vallès, 08290 Barcelona, Spain

HIGHLIGHTS

- PdCl₂ precursor (PdCl) enhances electron-donation to Pd nanoparticles (NPs).
- Carbon nanotubes (CNT) promote smaller Pd NPs and charge transfer to Pd NPs.
- Small Pd NPs with high electron density favor selectivity to olefins and stability.
- PdCl/CNT gives more than 80 % selectivity to olefins with H₂/chloroform = 10.
- Carbon nanofibers and Pd(NO₃)₂ favor bigger Pd NPs accelerating deactivation.

GRAPHICAL ABSTRACT



ARTICLE INFO

Keywords:

Hydrodechlorination
Chloroform
Olefins
CNT/CNF
Palladium
Electron density

ABSTRACT

The upgrading of wasted chloroform in hydrodechlorination for the production of olefins such as ethylene and propylene is studied by employing four catalysts (PdCl/CNT, PdCl/CNF, PdN/CNT, and PdN/CNF) prepared by different precursors (PdCl₂ and Pd(NO₃)₂) supported on carbon nanotubes (CNT) or carbon nanofibers (CNF). TEM and EXAFS-XANES results confirm that Pd nanoparticle size increases in the order: PdCl/CNT < PdCl/CNF ~ PdN/CNT < PdN/CNF, descending the electron density of Pd nanoparticles in the same order. It illustrates that PdCl-based catalysts show donation of electrons from support to Pd nanoparticles, which is not observed in PdN-based catalysts. Moreover, this effect is more evident in CNT.

The smallest and well-dispersed Pd nanoparticles (NPs) on PdCl/CNT with high electron density favor an excellent and stable activity and a remarkable selectivity to olefins. In contrast, the other three catalysts show

* Corresponding author.

E-mail address: luisa.gomez@uam.es (L. María Gómez-Sainero).

<https://doi.org/10.1016/j.jcis.2023.05.169>

Received 8 February 2023; Received in revised form 24 May 2023; Accepted 27 May 2023

Available online 29 May 2023

0021-9797/© 2023 The Authors. Published by Elsevier Inc. This is an open access article under the CC BY-NC license (<http://creativecommons.org/licenses/by-nc/4.0/>).

lower selectivity to olefins and lower activities which suffer strong deactivation due to the formation of Pd carbides on their larger Pd nanoparticles with lower electron density, compared to PdCl/CNT.

1. Introduction

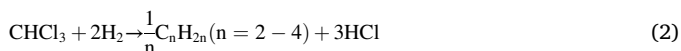
Chloromethanes (CMs) are a group of volatile organic compounds (VOCs) which have been widely used in the chemical industries owing to their unique physicochemical properties. Because of their high stability, high volatility and low flammability, they can be employed as solvents, degreasing agents, adhesive components, dry-cleaners, etc. [1]. Moreover, due to their high reactivity, CMs are also used in many synthetic industries as raw materials or intermediates [2]. As a result, tons of CMs are produced annually, leading to their high emissions into the atmosphere through evaporation and/or liquid discharges [1,2]. It has been confirmed that CMs are dangerous and harmful to the environment and human health. They are carcinogenic [3] and could destroy the ozone layer, promote the greenhouse effect and cause other environmental problems such as photochemical smog [4]. Therefore, in the last 40 years, extensive research has been devoted to control their emission [4].

Among the different solutions, catalytic hydrodechlorination (HDC) can be considered an exciting approach to degrade CMs since HDC can efficiently transform CMs into harmless non-chlorinated hydrocarbons under relatively low temperatures and atmospheric pressure. The literature contains several studies that convert waste dichloromethane (DCM) and chloroform (TCM) into methane (CH₄) through HDC employing suitable catalysts [5–8]. Nevertheless, the upgrading of CMs to light olefins becomes more attractive [9,10] since these light olefins, such as ethylene (C₂H₄), propylene (C₃H₆), and butylene (C₄H₈), are valuable hydrocarbons for the chemical industry. They are employed as key building-blocks chemicals in plastics, pharmaceuticals, and other fine chemical sectors.

In recent years, the dechlorination of monochloromethane (MCM) to produce olefins (Eq. (1)) has attracted increasing interest [11–16]. Structured zeolites like ZSMs and SAPOs were employed as catalysts for MCM dechlorination [11–14,16]. However, the application of this technology is limited by the strong deactivation of the zeolitic catalysts due to the oligomerization of hydrocarbons, which results in the formation and deposition of coke and the zeolite pore-blocking [11–14,16]. The relatively high reaction temperatures (400–500 °C) aggravate the coke formation [12,13].



Some previous studies [9,10] suggested that under suitable operating conditions, olefins production can be favored during the HDC of TCM (Eq. (2)). Besides, when compared to the MCM to olefins reaction, the HDC of TCM proceeds at a lower temperature (≤ 300 °C) and with hydrogen, which can result in higher catalytic stability [9].



Catalysts based on Pd, Ru and Rh have been investigated for olefins production by the HDC reaction of TCM [6,9,17]. Among them, under the same operating conditions and on a carbon support, Pd/C yields better selectivity to olefins than Ru/C and Rh/C [6]. Moreover, Fernandez-Ruiz et al. [9] used Pd-based catalysts supported on different activated carbons to study their ability to produce olefins by HDC of TCM. They found that mesoporous supports gave higher selectivity to olefins than microporous ones in the HDC of TCM reaction. On the other hand, considerable proportions of oxygen surface groups hindered olefins production, by promoting their hydrogenation, and catalyst deactivation. In that sense, mesoporous carbon materials like carbon nanofibers (CNF) and carbon nanotubes (CNT) appear to be suitable supports to overcome these problems. Although some good results have

been obtained in previous studies, development of new catalytic systems enhancing the selectivity to olefins and catalyst stability by a better control of their physicochemical properties, mainly metal particle size and oxidation state, are still needed.

In recent years, structured carbon supports like carbon nanotubes (CNT) and carbon nanofibers (CNF) have received much attention due to their high electrical conductivity and excellent mechanical and thermal properties [18–21]. Moreover, they offer increased accessibility to the active centers when used as catalytic supports. The absence of microporosity may also hinder the formation of carbon deposits over the active centers [22,23]. In addition, they usually show lower amounts of oxygen surface groups than activated carbons. Pd/CNF has been studied in the HDC of chlorobenzene, comparing its behavior to Pd catalysts supported on other carbon materials [22]. The high mesoporosity and strong metal-support interaction allowed Pd/CNF to exhibit the highest catalytic activity and stability. On the other hand, the CNT revealed some characteristic metal-support interactions leading to specific reactivity due to their unique structural features, such as the curvature, helicity and inner cavities [19]. Furthermore, the internal CNT channel could affect the selectivity to the expected products by shape-catalytic effects [19].

Despite these promising features, to the best of our knowledge, there is a lack of studies in the literature analyzing the HDC of TCM to obtain olefins using CNT or CNF. Thus, using these structured materials as catalytic supports for this reaction is quite an attractive novelty. The main purpose of this study is to evaluate the upgrading of waste TCM for producing light olefins by HDC, using palladium catalysts supported on CNT and CNF. Different Pd precursors will be used to obtain Pd active sites of varied nature, morphology, sizes, or electronic properties, ultimately determining catalyst activity.

2. Experimental

2.1. Catalysts preparation

Four palladium-based catalysts supported on CNT or CNF were prepared through incipient wetness impregnation. Two different Pd precursors were employed, PdCl₂ (>99 %) and Pd(NO₃)₂ (>99 %), supplied by Sigma-Aldrich. The multi-walled CNT (>90 %) presented diameters and lengths of 110–170 nm and 5–9 μm, respectively. The CNF (>98 %) possessed diameters and lengths of 100 nm and 20–200 μm, respectively. Both materials were used in powder form, as supplied by Sigma-Aldrich. First, the Pd precursor was dissolved in an acidic aqueous solution with an adequate concentration to obtain a nominal 1 wt% Pd loading on CNT or CNF. The as-prepared catalysts, denoted as PdCl/CNT, PdCl/CNF, PdN/CNT, and PdN/CNF (where PdCl and PdN refer to the precursor used, PdCl₂ or Pd(NO₃)₂, respectively), were dried at 100 °C (heating rate 20 °C/h) for 2 h. The dried catalysts were activated through reduction under a continuous 50 Ncm³ min^{−1} H₂ flow at 300 °C for 2 h. The H₂ (minimum purity: 99.999 %) was supplied by Nippon Gases.

2.2. Characterization

The porous texture of the catalysts was assessed through N₂ adsorption–desorption at −196 °C in Micromeritics equipment (Tristar II 3020). Before the analysis, the samples were outgassed at 150 °C for 12 h. The Brunauer - Emmett - Teller (BET) equation was employed to calculate the specific surface areas. The Pd entities' dispersions and nanoparticles (NPs) sizes were estimated from images acquired by transmission electron microscopy (TEM), employing a JEOL JEM-2100F

microscope operating at 200 kV with a resolution of 0.19 nm. The mean Pd NPs sizes were calculated by measuring >300 NPs in each catalyst sample.

The oxygen functional groups on the surface of CNT and CNF were determined by temperature-programmed desorption (TPD). The samples (0.1 g) were located inside a vertical quartz tube, heated under a continuous N₂ flow (1000 Ncm³ min⁻¹, minimum purity: 99.999 % supplied by Nippon Gases) up to 900 °C with a rate of 5 °C min⁻¹. The oxygen surface groups decomposed into CO₂ and/or CO were quantified using a Siemens Ultramat 23 Gas analyzer with a multi-layer infrared (IR) detector. The TPD peaks were deconvoluted using multiple Gaussian functions.

The crystalline structure of the catalysts was analyzed via X-ray diffraction (XRD) patterns obtained in an X'Pert PRO PANalytical diffractometer with an X'Celerator RTMS detector. The powdered samples were scanned by CuKα monochromatic radiation with $\alpha = 0.15406$ nm and a Ge mono filter. The scanning range (2 θ) was 10–90° with a scan step size of 0.0334. Signals were collected every 200 s.

The surface composition of the reduced catalysts was analyzed by X-ray photoelectron spectroscopy (XPS), employing a Multitechnique System of Physical Electronics 5700C with MgKα radiation (1253.6 eV). The compositions of the samples were determined by the general spectra recorded through scanning binding energy (BE) up to 1200 eV. C1s peak (284.6 eV) was employed as an internal standard to correct the BE changes aroused by sample charging. After smooth Shirley background subtraction, XPS spectra deconvolution was done employing mixed Gaussian–Lorentzian functions with a least-squares method. The relative atomic proportions of each element were calculated using areas of relative peaks deconvoluted from related core-level curves employing Wagner sensitivity factors [24].

X-ray spectroscopy (XAS) measurements were performed at CLAES beamline from ALBA Synchrotron, to study Pd atoms' electronic properties and local environment. Samples were auto-supported on a sample holder and placed into the solid–gas multipurpose cell available at the station for *in-situ* measurements. Pd K-edge XAS spectra were collected in fluorescence mode using a double-crystal Si(111) crystal monochromator. An MS spectrometer was connected to the outlet to follow the reaction and leak checking. The following experiments were performed: i) *in-situ* temperature-programmed reduction (TPR) in a mixture of 5 % H₂/N₂ from room temperature (RT) to 300 °C of the initial fresh catalysts, acquiring *in-situ* X-ray absorption near edge structure (XANES) along the treatment, after cooling to RT, Extended X-ray absorption fine structure (EXAFS) spectra were acquired; ii) after *in-situ* TPR, HDC of TCM reaction experiments (at 300 °C, with some higher TCM concentration than that used in laboratory experiments to accelerate the deactivation of catalysts) of selected catalysts, acquiring *in-situ* XANES along the reaction, followed by EXAFS acquisition after cooling to RT; iii) *ex-situ* EXAFS at RT of deactivated samples after reaction performed at the laboratory at 300 °C (1000 ppm_v of TCM in N₂ supplied by Nippon Gases at atmospheric pressure, space–time 0.2 kg h mol⁻¹ and H₂/TCM molar ratio = 50). Regarding EXAFS analysis, six consecutive EXAFS spectra were collected for averring before data analysis. The extraction and fitting of the $\chi(k)$ function were performed using the Viper code. Phase and amplitude functions for all single scattering paths were calculated by FEFF8 code. The averaged k³ $\chi(k)$ function was Fourier Transformed in the $\Delta k = 2.81$ –12.22 Å⁻¹ interval and the fits were performed in K-space. $\Delta R = 1.2$ –3.2 Å interval. Spectra normalization was performed with Athena program, part of Demeter package 0.9.26 [25].

2.3. Catalytic activity experiments

The catalytic activity of the reduced catalysts in the HDC of TCM reaction was evaluated in a continuous flow reaction system described elsewhere [26], consisting of a quartz fixed-bed micro-reactor (9 mm internal diameter) coupled to a gas-chromatograph (Varian 450-GC or

Agilent 7820A) with a capillary column (CP-SilicaPLOT, 60 m × 0.53 mm ID, Agilent, Madrid, Spain), employing a Flame Ionization Detector (FID) to analyze the evolution of the reactant and reaction products. The experiments were performed at atmospheric pressure, with 100 Ncm³/min total flow rate, a TCM inlet concentration of 1000 ppm_v diluted by N₂ supplied by Nippon Gases, and a reaction temperature of 300 °C. Different H₂/TCM molar ratios (50:1, 25:1, and 10:1) were tested. A space–time (τ) of 0.05 or 0.2 kg h mol⁻¹ was employed in the experiments.

The behavior of the catalysts in the HDC reaction was evaluated in terms of TCM conversion (X(TCM)) and selectivity to the different reaction products (S(i)), determined by Eqs. (3) and (4):

$$X(\text{TCM}) = \frac{C(\text{TCM})_{\text{in}} - C(\text{TCM})_{\text{out}}}{C(\text{TCM})_{\text{in}}} \times 100 \% \quad (3)$$

$$S(i) = \frac{C(i)_{\text{out}} \times N(\text{Carbon})_i}{C(i)_{\text{out}} \times N(\text{Carbon})_i + C(j)_{\text{out}} \times N(\text{Carbon})_j + \dots} \times 100 \% \quad (4)$$

where C(TCM)_{in} and C(TCM)_{out} are the concentrations of TCM at the inlet and outlet of the reactor, respectively, C(i)_{out} and C(j)_{out} are the concentrations of the products *i* and *j*, respectively, at the outlet of the reactor, and N(Carbon)_i and N(Carbon)_j refer to the number of carbon atoms in the products *i* and *j*, respectively.

3. Results

3.1. Catalytic activity tests

The activity of the catalysts was evaluated in the HDC of TCM. The products obtained were: CH₄ (C1); alkanes of more than one carbon atom (C1 + paraffins: ethane (C₂H₆), propane (C₃H₈), and traces of *n*-butane (n-C₄H₁₀)); olefins (C₂H₄, C₃H₆, and traces of 1-C₄H₈); and incompletely dechlorinated byproducts (MCM and DCM). The major products were CH₄, C₂H₄, C₂H₆, C₃H₆, and C₃H₈. Fig. 1(a) displays the evolution of TCM conversion obtained with different catalysts during the HDC reaction at 300 °C using an H₂/TCM molar ratio of 50. The evolution of the selectivities to the products during the reaction is presented in Fig. 2. The values obtained at the initial of each experiment are presented in Fig. 1(b). As can be observed, PdCl-based catalysts give rise to higher initial TCM conversion (PdCl/CNT (100 %) and PdCl/CNF (99 %)) than the PdN-based ones (PdN/CNT (88 %) and PdN/CNF (87 %)) (Fig. 1). For PdCl/CNT, TCM conversion practically remains unaltered during 12 h of reaction (final conversion: 99 %), while the other 3 catalysts suffer significant deactivation in different grade (final conversions: PdCl/CNF: 69 %; PdN/CNT: 58 %; PdN/CNF: 44 %). On the other hand, all selectivities remain practically stable on all catalysts during the reaction (Fig. 2). The olefins are the main products, showing the highest selectivity compared to other products for the four catalysts (Fig. 1(b)). On the PdCl-based catalysts, the selectivity to olefins is higher when using PdCl/CNT (70 %) than the PdCl/CNF (54 %), while on the PdN-based catalysts, the values of the selectivity to olefins are similar and lower than those on the PdCl-based catalysts (PdN/CNT: 48.8 % ~ PdN/CNF: 48.6 %). In addition, the selectivity to C1 + paraffins is similar or lower than the selectivity to methane on all catalysts (Selectivity to C1 + paraffins: PdCl/CNT: 15 %; PdCl/CNF: 18 %; PdN/CNT: 13 %; PdN/CNF: 5 %; Selectivity to methane: PdCl/CNT: 14 %; PdCl/CNF: 27 %; PdN/CNT: 37 %; PdN/CNF: 45 %). The selectivity to chloromethanes (DCM and MCM) is quite low with the four catalysts (PdCl/CNT: 1.6 %; PdCl/CNF: 1.4 %; PdN/CNT: 1.3 %; PdN/CNF: 1.3 %), showing dechlorination activities close to 100 %.

To improve the selectivity to olefins, different H₂ concentrations were tested. Since PdCl-based catalysts revealed better catalytic activity than PdN-based ones (Fig. 1), these catalysts were selected for this study. Fig. 3(a and c) display the evolution of TCM conversion during the HDC of TCM with different H₂/TCM molar ratios using PdCl/CNT and PdCl/

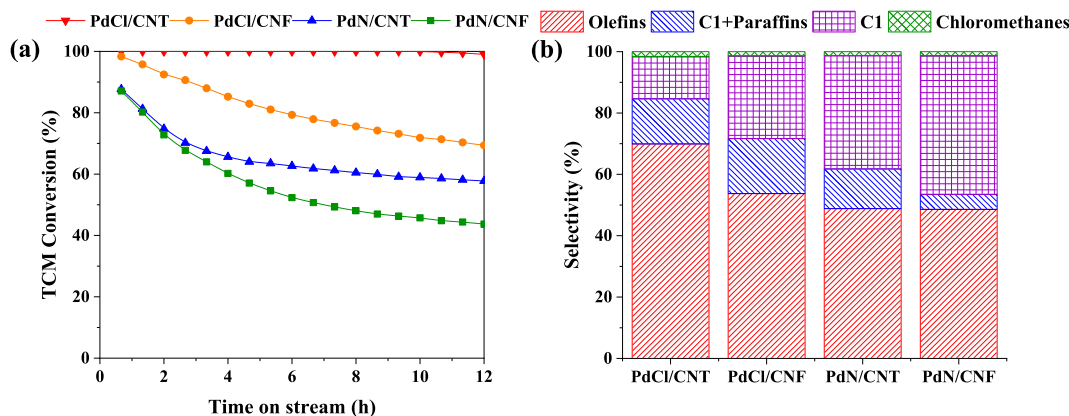


Fig. 1. Performance of the catalysts in the HDC of TCM, (a) Conversion of TCM, (b) Initial selectivity to reaction products. ($\tau = 0.2 \text{ kg h mol}^{-1}$; $T_{\text{reaction}} = T_{\text{reduction}} = 300^\circ\text{C}$; $\text{H}_2/\text{TCM} = 50$; each experiment was repeated 3 times with an estimated error lower than 5 %).

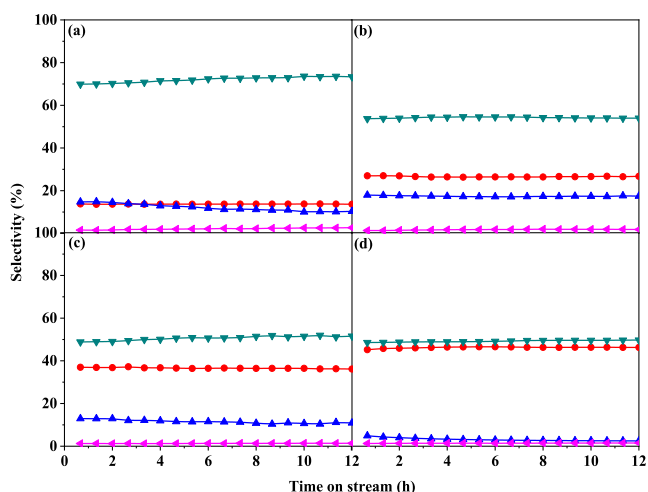


Fig. 2. Evolution of the selectivities to the products in HDC of TCM reactions: (a) PdCl/CNT; (b) PdCl/CNF; (c) PdN/CNT; (d) PdN/CNF. (▼: selectivity to olefins; ▲: selectivity to paraffins; ●: selectivity to methane; ◄: selectivity to MCM. $\tau = 0.2 \text{ kg h mol}^{-1}$; $T_{\text{reaction}} = T_{\text{reduction}} = 300^\circ\text{C}$; $\text{H}_2/\text{TCM} = 50$; each experiment was repeated 3 times with an estimated error lower than 5 %).

CNF, respectively. The evolution of product selectivities during the reaction, and their values at the initial of the experiments, are presented in Fig. 3(b and d) and 4, respectively. As depicted, when reducing H_2/TCM molar ratio, PdCl/CNT initial conversion remains complete. After a steady-state period, a slight decrease in TCM conversion is observed, which is more pronounced when reducing H_2/TCM molar ratio, while the selectivity to olefins significantly increases with high stability (Fig. 3 (a and c) and 4(a, b, and c)). In contrast, the reduction of the H_2 proportion gives stronger deactivation to PdCl/CNF, which seems affect significantly to the enhancement of the selectivity to olefins, especially when reducing the H_2/TCM molar ratio from 25 to 10 (Fig. 3(c and d) and 4(e and f)). Regarding the other products, in general when reducing the H_2 proportion, in both catalysts, the selectivities to CH_4 and C1 + paraffins decrease, whereas the selectivity to chloromethanes increases. Their selectivities are much more influenced by the reduction of H_2 proportion over PdCl/CNF than over PdCl/CNT.

In all cases (Figs. 2 and 4), the selectivity to C1 + paraffins is maximum at the beginning of the reaction; then, some slight decreases occur while somewhat increases take place in the selectivity to olefins. The selectivities to methane and MCM remain practically stable during the reaction.

As previously stated, the PdCl/CNT shows a complete initial TCM

conversion which remains practically stable during the reaction (Fig. 1 (a) and 3(a)). To confirm its high stability, a lower space-time value is applied ($\tau = 0.05 \text{ kg h mol}^{-1}$) with an $\text{H}_2/\text{TCM} = 50$. The PdCl/CNF is also tested as a counterpart. As shown in Fig. 5(a), with the lower space-time, the PdCl/CNT offers an initial TCM conversion of ca. 61 %, which also remains practically stable during the reaction; only a slight deactivation is observed. On the other hand, the PdCl/CNF shows a much lower initial TCM conversion (ca. 45 %) and suffers a strong deactivation; the final TCM conversion drops to a value of ca. 25 % (Fig. 5(a)). Herein, the high stability of PdCl/CNT seems to be confirmed through the reduction of space-time. In addition, the distribution of the initial selectivity to the products of both catalysts shown in Fig. 5(b) is similar to the obtained with a higher value of space-time (Fig. 1 (b) and 3 (b and d)).

3.2. Characterization results

Fig. 6 represents the N_2 adsorption-desorption isotherms of the catalysts, while the BET surface areas of all the catalysts are listed in Table 1. According to the IUPAC classification, all the isotherms shown in Fig. 6 correspond to type II materials [27], characteristic of mesoporous materials with low microporosity contribution, as indicated by the low N_2 adsorption at low relative pressures. The presence of the hysteresis loops can be ascribed to the nitrogen capillary condensation in slit-shaped mesopores. Regardless of the palladium precursor, the catalysts supported on the same support, CNT or CNF, present similar isotherms and surface areas (S_{BET}) around 100 or $25 \text{ m}^2 \text{ g}^{-1}$, respectively (Table 1). The higher surface areas of the catalysts based on CNT can be probably due to their inner cavity. No significant changes are observed in the porosity of the used catalysts (not presented), suggesting that no evident formation of carbonaceous deposits occurred during the reaction.

Table 2 displays the concentration of surface oxygen functional groups of the four catalysts and the supports, CNT and CNF, obtained from the deconvolution of the TPD profiles shown in Figs. S1 and S2 (Supplementary material), based on previous reports [28–30]. The peaks appearing in the CO_2 profiles are identified as carboxylic acid ($270\text{--}350^\circ\text{C}$), carboxylic anhydride ($440\text{--}590^\circ\text{C}$), and lactone ($620\text{--}710^\circ\text{C}$). Meanwhile, the deconvoluted peaks from CO profiles correspond to carboxylic anhydride ($440\text{--}590^\circ\text{C}$), phenol ($620\text{--}680^\circ\text{C}$), ether ($740\text{--}770^\circ\text{C}$), and carbonyl/quinone ($850\text{--}900^\circ\text{C}$).

CNT demonstrates a wider variety and higher concentration of surface oxygenated functional groups than CNF (Table 2). The acids used for catalysts preparation promote increased oxygenated functional groups concentration [31] after impregnation, HNO_3 leading to a higher concentration of oxygenated functional groups than HCl, especially of carbonyl/quinone and carboxylic acid species (Table 2). In the end, both

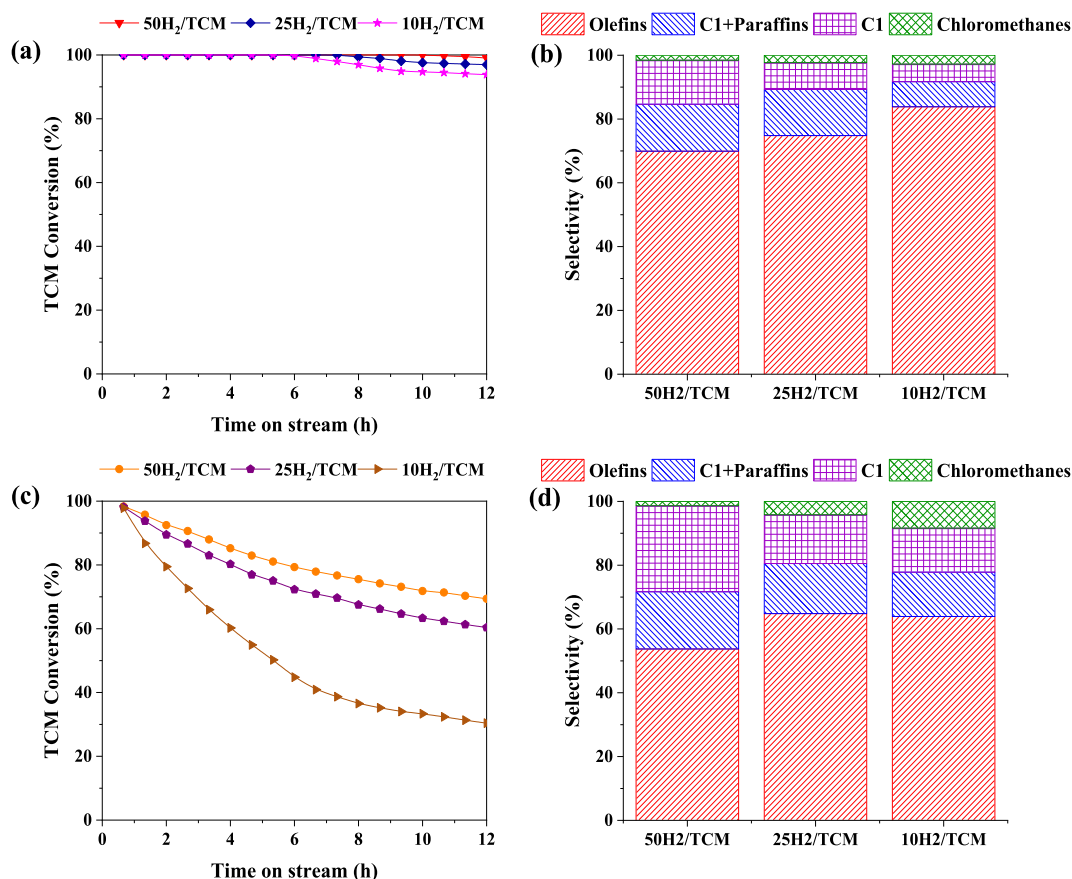


Fig. 3. Influence of H_2/TCM ratio in the HDC of TCM using different supports: (a) Conversion of TCM and (b) Initial selectivity to reaction products using PdCl/CNT; (c) Conversion of TCM and (d) Initial selectivity to reaction products using PdCl/CNF. ($\tau = 0.2 \text{ kg h mol}^{-1}$; $T_{\text{reaction}} = T_{\text{reduction}} = 300^\circ\text{C}$; each experiment was repeated 3 times with an estimated error lower than 5 %).

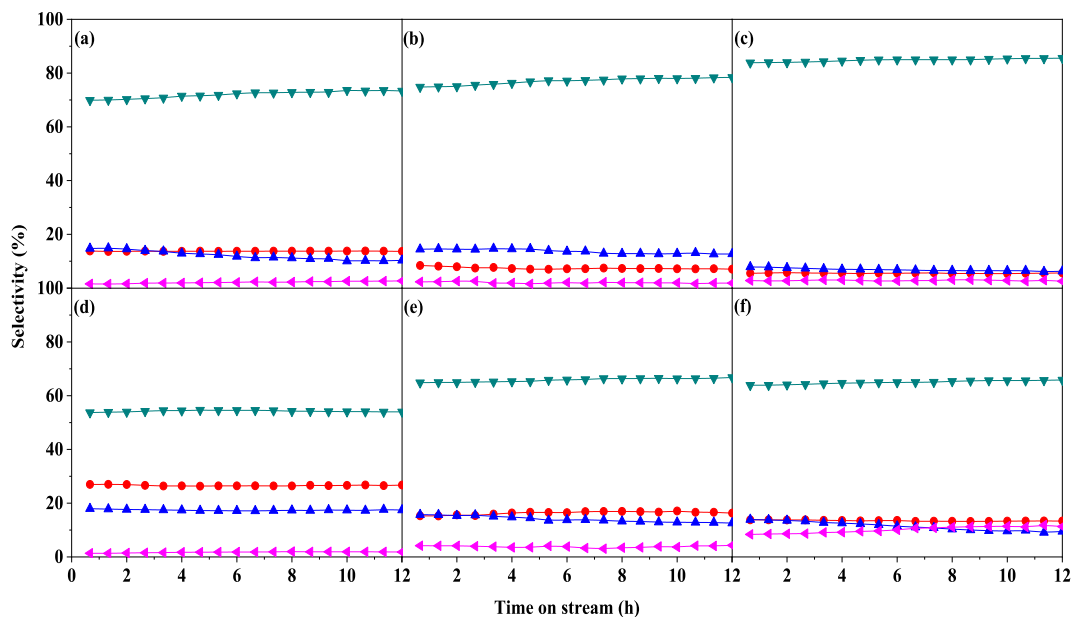


Fig. 4. Evolution of the selectivities to the products in HDC of TCM reactions: (a) 50 H_2/TCM , (b) 25 H_2/TCM , and (c) 10 H_2/TCM using PdCl/CNT; (d) 50 H_2/TCM , (e) 25 H_2/TCM , and (f) 10 H_2/TCM using PdCl/CNF. (▼: selectivity to olefins; ▲: selectivity to paraffins; ●: selectivity to methane; ◀: selectivity to MCM. $\tau = 0.2 \text{ kg h mol}^{-1}$; $T_{\text{reaction}} = T_{\text{reduction}} = 300^\circ\text{C}$; each experiment was repeated 3 times with an estimated error lower than 5 %).

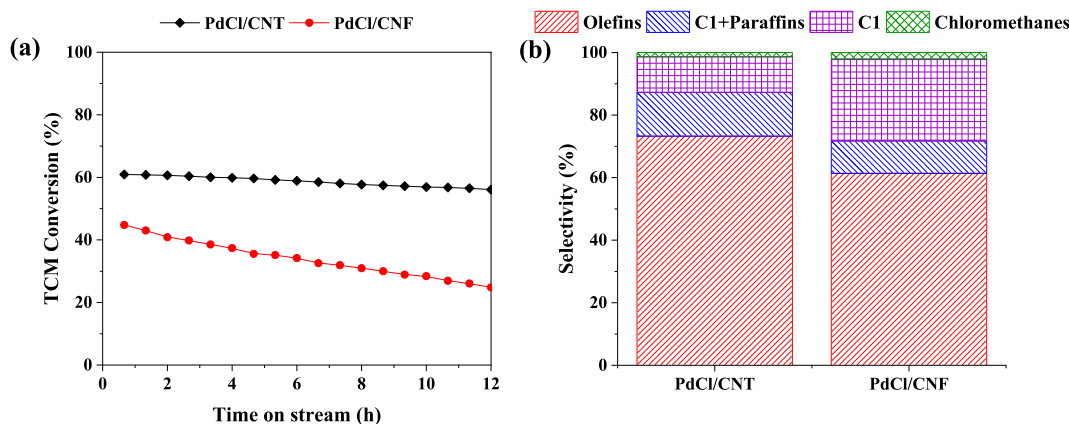


Fig. 5. Performance of the PdCl/CNT and PdCl/CNF in the HDC of TCM with a lower value of τ , (a) Conversion of TCM, (b) Initial selectivity to reaction products. ($\tau = 0.05 \text{ kg h mol}^{-1}$; $T_{\text{reaction}} = T_{\text{reduction}} = 300^\circ\text{C}$; $\text{H}_2/\text{TCM} = 50$; each experiment was repeated 3 times with an estimated error lower than 5 %).

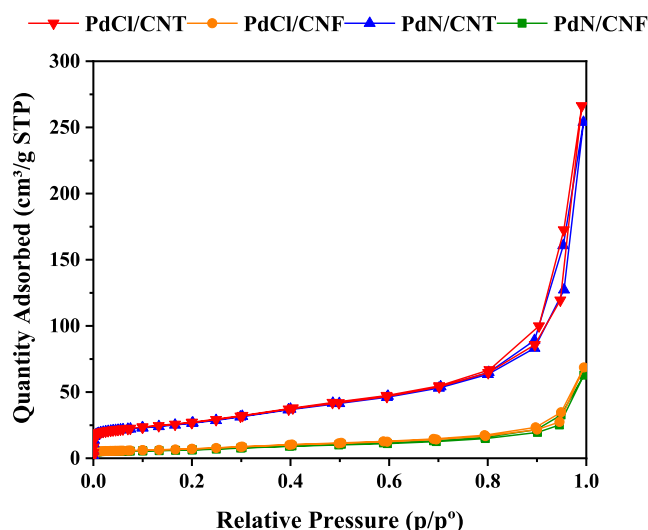


Fig. 6. N_2 adsorption-desorption isotherms of the catalysts at -196°C .

Table 1
Summary of physicochemical properties of the catalysts.

Catalyst	S_{BET} ($\text{m}^2 \text{g}^{-1}$)	Mean Pd NP size (nm)	XPS Pd species surface distribution	
			Pd^0 (%)	Pd^{n+} (%)
PdCl/CNT	96	2.5	79.7	20.3
PdCl/CNF	25	3.7	84.3	15.7
PdN/CNT	94	4.3	63.6	36.4
PdN/CNF	22	8.6	67.3	32.7

Table 2
TPD analysis results: total amounts of CO and CO_2 ; distribution of oxygen functional groups obtained from deconvolution of TPD profiles.

Sample	CO_2 ($\mu\text{mol g}^{-1}$)	CO ($\mu\text{mol g}^{-1}$)	carboxylic acid ($\mu\text{mol g}^{-1}$)	phenol ($\mu\text{mol g}^{-1}$)	ether ($\mu\text{mol g}^{-1}$)	lactone ($\mu\text{mol g}^{-1}$)	carboxylic anhydride ($\mu\text{mol g}^{-1}$)	carbonyl/quinone ($\mu\text{mol g}^{-1}$)
PdCl/CNT	410	1412	23	282	551	47	501	386
PdCl/CNF	289	632	29	87	13	61	186	212
PdN/CNT	424	1493	143	696	206	48	229	693
PdN/CNF	525	1174	52	21	444	107	294	549
CNT	351	647	48	31	200	55	208	285
CNF	252	264	19	36	–	14	150	47

materials form different oxygenated groups preferably.

Pd NPs sizes distributions and some representative TEM images of the reduced catalysts are shown in Fig. 7. The mean NPs sizes are summarized in Table 1. As observed, using PdCl₂ as precursor and CNT as support promotes smaller NPs sizes.

The XRD patterns of reduced and used (in the HDC of TCM with $\text{H}_2/\text{TCM} = 50$) catalysts are shown in Fig. S3 (Supplementary material). According to previous reports, the characteristic peaks corresponding to the structured carbon supports (CNT and CNF) are identified [32,33].

No signals related to Pd species are observed in the XRD patterns of PdCl/CNT and PdCl/CNF (Fig. S3), probably due to their relatively small NPs sizes. On the PdN-based catalysts patterns, a peak corresponding to Pd(111) structural facet in metallic Pd crystallite appears at $2\theta = 40.1^\circ$ [34], in agreement with the bigger NPs sizes observed by TEM for these catalysts (Fig. 7). The positions and intensities of the Pd peaks in the PdN-based catalysts are compared in Fig. 8. The Pd peak in PdN/CNT is smaller than in PdN/CNF, confirming the TEM results (Table 1). In the used catalysts, the Pd peaks are displaced to lower scattering angles ($2\theta = 39.2^\circ$), probably due to the formation of palladium carbide (PdC_x) during the reaction [5]. Carbon atoms from different carbon-containing molecules involved in the HDC reaction may be incorporated into the Pd lattice, increasing the lattice distance and shifting the Pd peaks to lower angles.

The Pd 3d region of the XPS profiles of the reduced catalysts is displayed in Fig. 9. In all cases, Pd 3d signal can be deconvoluted into a doublet (Pd 3d_{5/2} and Pd 3d_{3/2}) employing a 0.66 area ratio associated with d orbital, and a doublet separation value of 5.26 eV [35]. For the Pd 3d_{5/2} zone, the peak centered at nearly 335.5 eV can be considered as zero-valent Pd (Pd^0), and the one at around 338.0 eV can be related to electron-deficient Pd (Pd^{n+}) [35]. The atomic proportions of the two identified Pd species on the surface are summarized in Table 1. All the catalysts show most of the surface Pd in a zero-valent state. However, the proportion of Pd^{n+} is somewhat higher when using nitrate as the

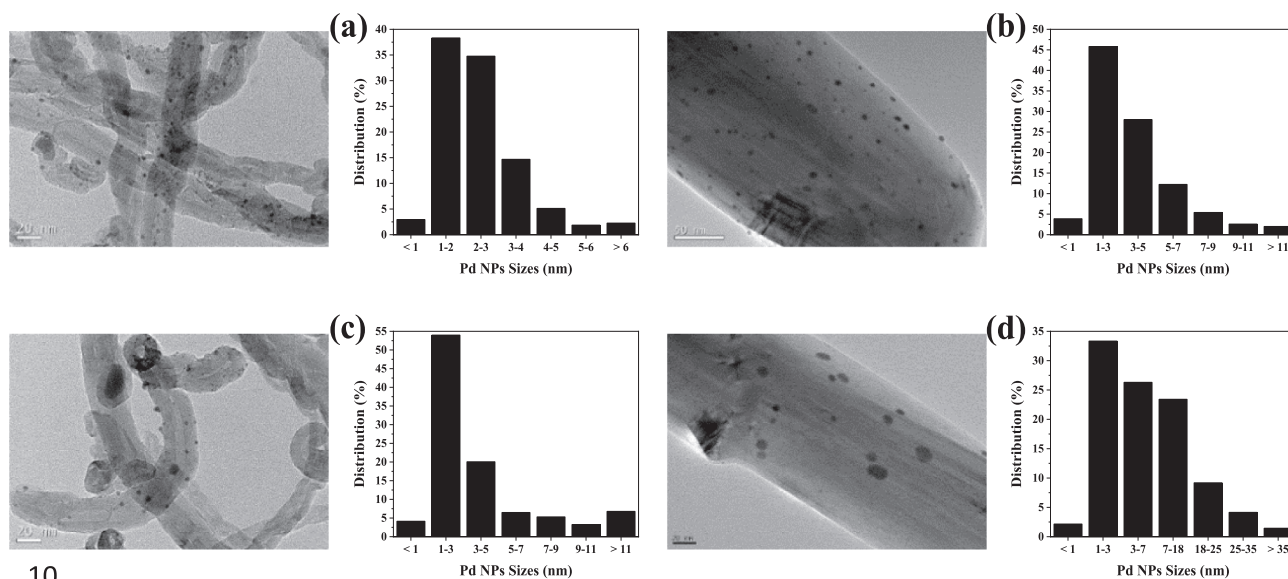


Fig. 7. Representative TEM images and Pd NPs sizes distribution of the reduced catalysts: (a) PdCl/CNT; (b) PdCl/CNF; (c) PdN/CNT and (d) PdN/CNF.

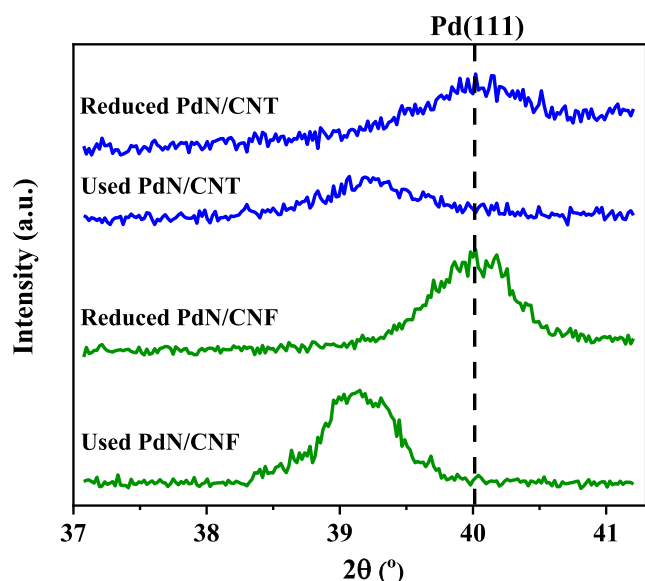


Fig. 8. XRD patterns of reduced and used PdN-based catalysts.

precursor and slightly higher for CNT than for CNF support, which can be ascribed to the higher concentration of oxygen functional groups (Table 2) that promote metal-support interactions [36].

The XANES spectra of the Pd-species obtained after H₂ treatment are displayed in Fig. 10. For all samples, XANES shape (edge position and continuum resonance, CR, characteristics) is unequivocally ascribable to Pd metallic species in an fcc-matrix [37]. However, there are some differences with the typical pure metal XANES spectrum (Pd-foil reference) concerning the energy position of the edge and the CRs, and their intensity. Differences are observed regarding the global intensity of the CRs, being lower for the samples obtained from the chloride precursor than for the samples obtained from nitrate. This can be explained on the basis of Pd NPs sizes variations that appears to be lower (analyzing the height and width of the CRs [38]) for the PdCl/CNT < PdCl/CNF ~ PdN/CNT < PdN/CNF, in good correlation with what was observed in the TEM analysis.

The catalysts prepared using the chlorinated precursor show lower Pd K-edge energy position values than the reference (spectra first

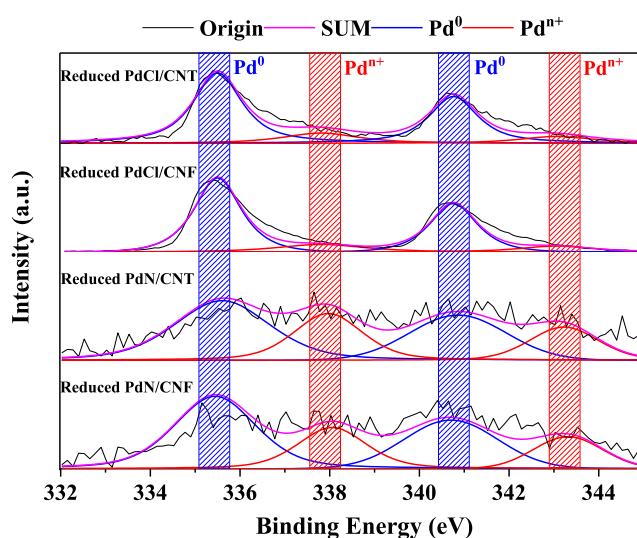


Fig. 9. XPS profiles of the reduced catalysts.

derivative presented in Fig. 10-inset). This suggests a higher electron density of those Pd centers than in the foil. In addition, for PdCl/CNT, where the red-shift was greater, there is a significant intensity decrease for the 5sp (ca. 24365 eV) and 4f (ca. 24395 eV) CRs. Their intensity can be related to a lower density of unoccupied states, agreeing with the higher electron density indicated above. On the contrary, the PdN/CNF sample presents a slightly higher edge position than the foil, while for PdN/CNT it was similar. Thus, Cl presence is implied to significantly affect the electronic properties of the Pd entities in these carbon-based systems, affecting the reactivity of the Pd centers. But the exact role Cl may play in developing different types of Pd catalysts strongly depends on the support nature where Pd is deposited. The results suggest that CNT support can transfer more electrons into the empty Pd states in the PdCl/CNT which presents small Pd NPs.

In addition, differences among Pd samples can be explained based on variations in NPs sizes, which, on the other hand, is also support-depending. EXAFS spectra were acquired for all the reduced samples to investigate the local structure around the Pd atoms. The Fourier transforms of the Pd k³-weighted spectra are shown in Fig. 11, and the structural parameters determined from the curve fitting are summarized

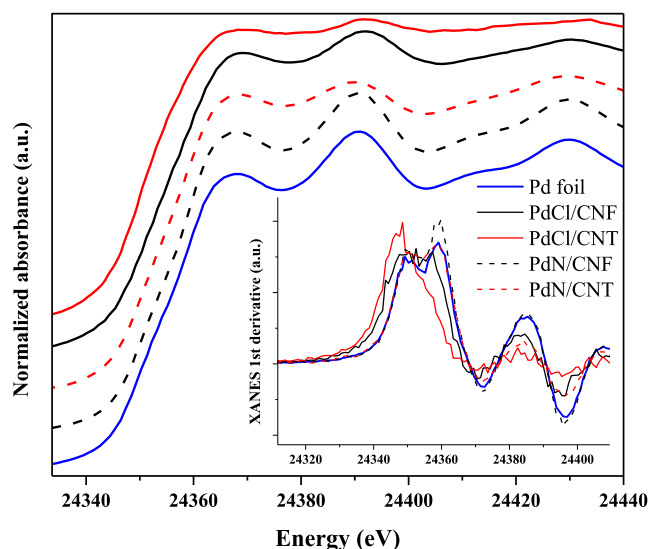


Fig. 10. Pd K-edge XANES spectra of the reduced samples PdCl/CNT, PdCl/CNF, PdN/CNT, PdN/CNF, and the Pd foil reference. The figure inset shows the first derivative of the XANES spectra.

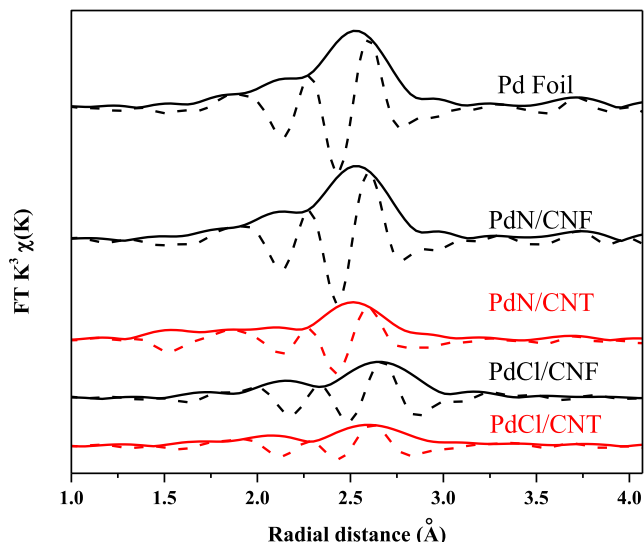


Fig. 11. K^3 -weighted modulus and imaginary part of the Fourier transform of Pd K-edge EXAFS spectra at room temperature corresponding to the reduced catalyst: PdCl/CNT, PdCl/CNF, PdN/CNT, and PdN/CNF. The Fourier transform of the Pd foil is also shown as a reference.

in Table S1 (Supplementary material).

The EXAFS data show that Pd bulk is present as Pd metallic species for all catalysts. The feature at ca. 2.75 Å corresponds to the Pd – Pd atomic distance in the first coordination shell of bulk Pd metal. For fcc-metal systems, the coordination number of this Pd – Pd path, N1, can be related to the number of atoms per average Pd NPs [39]. Thus, the average Pd NPs diameters were estimated assuming a spherical morphology: 1, 2, 2–3, and > 4 nm for PdCl/CNT, PdCl/CNF, PdN/CNT, and PdN/CNF, respectively ($\pm 10\%$ error in the value of N1 Pd-Pd). The EXAFS studies confirmed the same sequence of mean Pd NPs sizes (PdCl/CNT < PdCl/CNF ~ PdN/CNT < PdN/CNF) observed by TEM (Table 1). The discrepancies in the values are because the microscopy overestimates the average sizes and leaves out Pd NPs with sizes below its resolution, while the EXAFS averages all. Regardless of the precursor used, the support CNT favors the formation of smaller Pd NPs than CNF, probably due to its larger surface area (Table 1). However, in all cases,

the nitrate precursor leads to larger Pd NPs than the chlorine precursor, since PdCl/CNF continues to have smaller Pd NPs sizes than PdN/CNT even though the support area is four times smaller.

Since the PdCl-based catalysts revealed better catalytic activity than the PdN-based ones (Fig. 1) and the role played by Cl in the development of different types of Pd catalysts strongly depends on the support nature, PdCl/CNT and PdCl/CNF were selected for the *in-situ* and *operando* studies.

Fig. 12(a and b) show the evolution of XANES spectra during TPR in H_2 up to 300 °C. At the same time, Fig. 12(c) depicts the evolution of oxidized and reduced species as a function of temperature during TPR. As observed, Pd in CNF begins to reduce at lower temperatures, being the process more gradual. On CNT, Pd is reduced at higher temperatures (45 °C of difference) and once the process has started takes place somewhat faster than on CNF.

After TPR, at the same temperature (300 °C), a reaction gas mixture was introduced for an *operando* study. Significant differences were found in the behavior of both chlorinated catalysts. The XANES results of PdCl/CNF show that the maximum of the continuous resonance feature (1 s-4f;pf) shifts to lower energies under reaction conditions (Fig. 13). Since the edge position corresponds to Pd metallic specie and there are no more modifications during the reaction, the changes can be related to the lattice distances expansion considering the $1/R^2$ rule [40,41]. The Pd affinity to form hydride species in the presence of H_2 is well-known and reported [42]. However, these species are not stable over 120–150 °C. Therefore, this lattice expansion suggests the formation of PdC_x species under these conditions, produced by the inclusion of C atoms within the metal lattice.

Conversely, PdCl/CNT XANES spectra did not suffer any change during the experiment under HDC of TCM and remained stable under reaction conditions (not shown). This result (under a more harmful environment) sharpens this catalyst's high stability. However, the formation of PdC_x in the PdCl/CNF sample was almost instantaneous as soon as TCM was introduced and may explain the stronger deactivation observed for PdCl/CNF catalyst compared to PdCl/CNT, whose activity remained stable under the reaction conditions. The PdC_x formation was also observed at the initial stages of HDC of DCM reaction using a Pd-based catalyst in our previous catalytic deactivation study [43].

4. Discussion

As stated in Section 3.1. and seen in Table 1 and Fig. 7, when comparing the catalysts with the same Pd precursor, those supported on CNT show smaller Pd NPs (mean NP size: PdCl/CNT: 2.5 nm; PdN/CNT: 4.3 nm), and better distribution on the support than those based on CNF (mean NP size: PdCl/CNF: 3.7 nm; PdN/CNF: 8.6 nm). Besides the contribution of the higher surface area of CNT support, which allows a better dispersion of Pd NPs leading to smaller NPs sizes, XANES-TPR results (Fig. 12) show a stronger interaction of Pd with CNT support that shifts the reduction process to higher temperatures, retarding Pd NPs nucleation and growth processes. Thus, smaller Pd NPs sizes are reached in CNT than in CNF.

On the other hand, PdN-based catalysts present bigger Pd NPs than their chlorinated counterparts, PdCl-based catalysts (Fig. 7, Table 1). This can be ascribed to the higher concentration of carboxylic acid groups on the PdN-based catalysts (Table 2). According to the literature [44], carboxylic acid groups negatively influence the Pd nucleation process during H_2 treatment due to their lower thermostability compared to other oxygenated groups. They thermally decompose at 270–350 °C [29]. In this study, before the reaction, the catalysts were reduced at 300 °C, when the carboxylic acid groups would decompose, facilitating Pd NPs agglomeration (enlargement of NPs observed by TEM, Fig. 7). Consequently, a higher amount of larger Pd NPs is observed for PdN-based catalysts. The lower concentration of carboxylic acid groups (Table 2), higher surface area (Table 1), and stronger interaction of Pd NPs with the support promote smaller Pd NPs for PdCl/

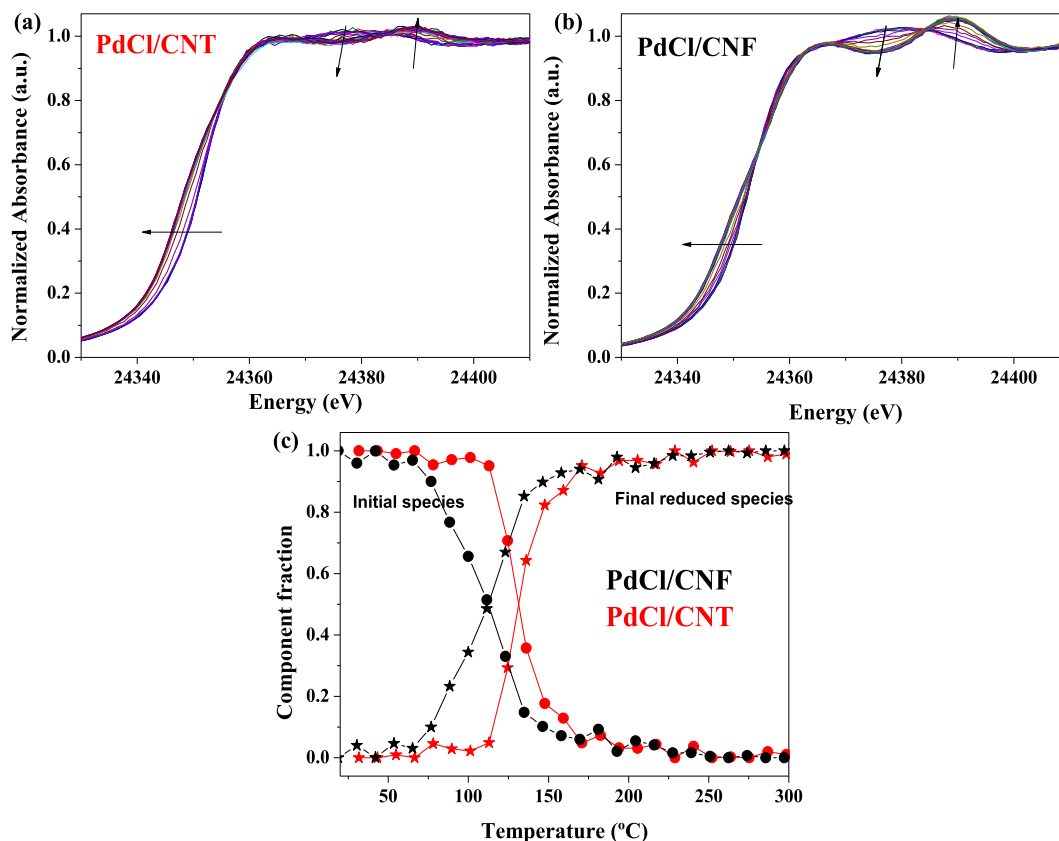


Fig. 12. Set of Pd K-edge XANES spectra acquired during in situ H_2 TPR for a) PdCl/CNF and b) PdCl/CNT. c) Fraction evolution of initial (●) and final species (○) during TPR in H_2 for PdCl/CNF (black) and PdCl/CNT (red). (For interpretation of the references to colour in this figure legend, the reader is referred to the web version of this article.)

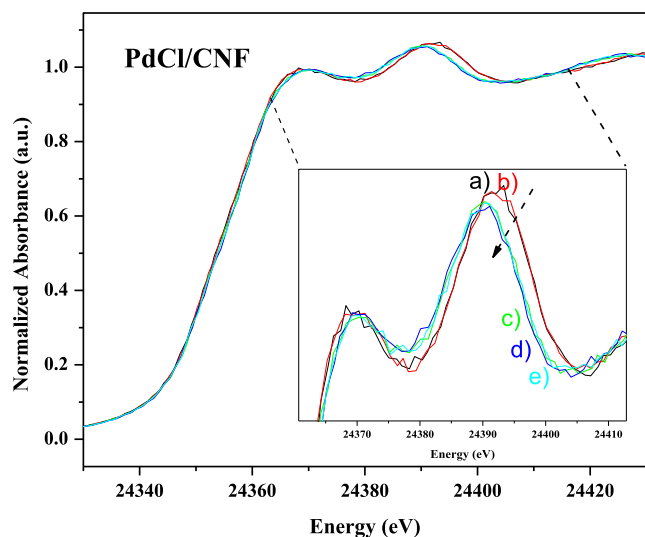


Fig. 13. Pd K-edge XANES spectra during HDC of TCM reaction conditions at 300 °C. (a) In H_2 before introducing reaction gas mixture, (b) 1st spectrum, (c) 2nd, (d) 3rd and (e) last spectrum after 2 h under reaction conditions for PdCl/CNF.

CNT.

The EXAFS studies (Fig. 11) confirm the increasing order of mean Pd NPs sizes (PdCl/CNT < PdCl/CNF ~ PdN/CNT < PdN/CNF) in agreement with TEM analysis results (Fig. 7, Table 1). Moreover, both XANES and EXAFS data reveal that Pd presents a bulk metallic state for all catalysts after H_2 treatment (Figs. 10 and 11), although differences in

electronic properties are observed.

XPS data indicate the presence of some partially oxidized centers on the surface of catalysts powders. However, when studying the electronic properties of the whole catalyst samples through the XANES analysis, only a minor part of Pd in PdN/CNF is electro-deficient (red shift observed in the edge position), not finding electron-deficient Pd centers in PdCl/CNT, PdCl/CNF, and PdN/CNT, since XANES fingerprints comprise all Pd atoms in the sample (not only the surface).

Conversely, the increase in electron density revealed by XANES (Fig. 10) on PdCl-based samples is probably due to a charge transfer from the carbon support structure to the 4d-band of Pd that affects Pd adsorption strength. According to the literature [45–49], a different electron density exists between the outer and inner surfaces of the CNT due to the shift of π electrons from the concave inner to the convex outer surface. More delocalized π electrons are preferably concentrated on the CNT outer surface, which favors the donation of electrons to the Pd NPs. On the other hand, since CNF is an ordered structural carbon material, some free electrons will also be present on its surface [45]. Accordingly, when comparing PdCl/CNT and PdCl/CNF, the charge transfer is more evident in PdCl/CNT. These electronic effects also increased when decreasing metal particle size [50], which would also contribute to explaining the higher electron density of PdCl/CNT (with the smallest Pd NPs sizes), not being observed for PdN/CNT and PdN/CNF (Figs. 10 and 11). For these catalysts, TEM (Table 1) and EXAFS (Fig. 11) results probed the existence of bigger Pd NPs than in PdCl counterparts. However, apart from the structure effects, the Cl ions from Pd-precursor may also modify the electronic properties of the support, favoring an electron-donation from the support to the final deposited Pd NPs. This is evidenced since, conversely than for PdN/CNT, despite having similar Pd NPs mean size, the electron-donation from the support is observed for PdCl/CNF (Fig. 10-inset).

The combination of the higher electron-donation of CNT support, the chloride precursor, and the smallest Pd NPs of PdCl/CNT (Table 1 and Fig. 11) leads to the higher electron density of Pd in this catalyst (Figs. 10 and 12).

The catalytic activity results show that PdCl/CNT achieves a 100 % and ca. 61 % conversions of TCM with $\tau = 0.2$ and $0.05 \text{ h kg mol}^{-1}$, respectively, which practically remains unaltered for 12 h of reaction (Fig. 1(a) and 5(a)). This absence of deactivation correlates with the high stability observed for Pd entities in this catalyst, inferred from the analysis of the *operando* XANES during HDC of TCM reaction (the XANES spectrum of the PdCl/CNT remained stable during the reaction). The excellent activity and stability of PdCl/CNT can be attributed to its smallest and well-distributed Pd NPs (Table 1, Figs. 7 and 11), which also prevents the formation of PdC_x , usually taking place in bigger Pd NPs, facilitating the deactivation of the catalysts [5,51]. On the contrary, the appearance of PdC_x has been observed in the other three catalysts (by the *operando* XANES under the HDC of TCM reaction study for PdCl/CNF (Fig. 13) and by XRD for PdN/CNT and PdN/CNF (Fig. 8)), in good agreement with their more significant loss of activity (Fig. 1).

Thus, the deactivation of these three catalysts (PdCl/CNF, PdN/CNT and PdN/CNF) shown in Fig. 1 can be mainly ascribed to their larger Pd NPs (which promote the formation of PdC_x) compared to PdCl/CNT (Fig. 7). Besides, the deactivation degree of the catalysts increases when decreasing Pd electron density (Figs. 1 and 10), this last following the order: PdCl/CNT > PdCl/CNF > PdN/CNT > PdN/CNF. PdN/CNF even shows some electron-deficient character (Fig. 10). A previous study with activated carbon-supported catalysts found the same relationship between Pd electron density and catalyst stability [37]. The active centers with lower electron density could be more strongly poisoned by the adsorption of TCM intermediates, reaction products, or both. Regardless of Pd precursor effects, the catalysts supported on CNF show lower stability than their counterpart on CNT, suggesting a possible influence of BET surface area on the stability of the catalysts.

All the catalysts demonstrated high dechlorination ability since the selectivity to chloromethanes (DCM and MCM) is relatively low during the reaction, ranging from 1.3 to 3.5 % (Fig. 1(b)). The proportion of methane, larger paraffins, and olefins differ depending on the catalyst. HDC is a reductive reaction that uses H_2 as the reducing agent. In this case, the reduction involves the removal of the three adjacent halogen atoms on the same alkane (CHCl_3), leading to the formation of C–H bonds or an additional C–C bond. Electrons are transferred to the organochlorine molecule, which decomposes to produce the corresponding hydrocarbon (hydrogen atoms substituting the original chlorine atoms) and free Cl ions (reaction in which the elements of hydrogen chloride are removed from a molecule). Based on other experimental evidence, it has been proposed that under mildly reducing conditions, halogenated methanes and ethanes reduction is initiated by a dissociative one-electron transfer, leading to bond dissociation and the formation of an extremely reactive radical [52,53]. The dechlorination of chloroalkanes can thus be formulated according to Eq. (5) [52]:



After, hydrogenolysis can take place, with the inclusion of the H atom to the alkane, or C–C coupling reaction, giving rise to hydrocarbons with a higher chain.

Some theoretical studies [6,54,55] confirmed that CH_4 is the most favorable and stable product in the HDC of chloromethanes reactions due to its lowest formation energy. Herein, the formation of CH_4 may always accompany the HDC of TCM (Fig. 1(b)). However, the higher electron density of the metallic Pd centers may be a facilitator for the reductive dehalogenation of the chloro-organic, favoring coupling reactions. In previous theoretical studies [54,56], the increase of electron density of Pd was found to enhance chloromethanes' dissociative adsorption while disfavoring that of H_2 . Therefore, C1/C1 + formation appears to be related to the electron density of Pd NPs in each catalyst.

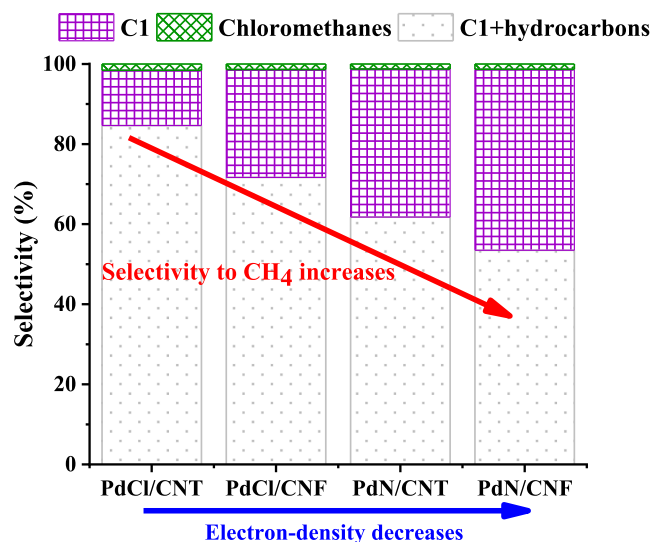


Fig. 14. Relationship between the selectivity to CH_4 (C1) and the electron-density of the catalysts. ($\tau = 0.2 \text{ kg h mol}^{-1}$; $T_{\text{reaction}} = T_{\text{reduction}} = 300^\circ\text{C}$; $\text{H}_2/\text{TCM} = 50$).

The selectivity to CH_4 enhances when decreasing Pd electron density (Fig. 14). Therefore, although Pd NPs sizes are similar on PdCl/CNF and PdN/CNT (Figs. 7 and 11), the distribution of selectivities to the main products changes significantly. The lower electron density and even the formation of Pd^{n+} appear to favor the formation of CH_4 via stronger interaction with the reactants. In addition, the generation of Pd^{n+} may be assisted by the formed PdC_x in the three catalysts (PdCl/CNF, PdN/CNT, and PdN/CNF). PdC_x is formed by the incorporation of C atoms into the Pd lattice, resulting in the expansion of the Pd lattice, which means that the distance between the Pd atoms becomes longer in the Pd crystals due to the interference of C atoms, resulting in lowering the catalytic activity of the Pd phase [5]. The C–C bonds may be hardly generated over PdC_x since they need to interact with at least 2 nearing Pd atoms. However, some mono-carbon products like CH_4 may be formed. Another theoretical study [57] reveals that the PdC_x shows higher hydrogenation ability than the clean Pd phase.

On the other hand, PdCl/CNT shows much higher selectivity to olefins (70 %) than the other 3 catalysts whose selectivities to olefins are: PdCl/CNF (54 %) > PdN/CNT (48.8 %) ~ PdN/CNF (48.6 %) (Fig. 1 (b)). This can be attributed to its smaller Pd NPs (Table 1) and the remarkable higher electron density of Pd NPs in PdCl/CNT (Fig. 10). These properties have demonstrated to promote the formation of unsaturated hydrocarbons [9,58]. On the contrary, the hydrogenation of olefins to paraffins could be favored over Pd^{n+} species [9,46] through the stronger interaction with the formed olefins [9]. For PdCl/CNT, with the highest charge of Pd centers, olefins production notably increases (Fig. 3(b)).

It is clear that olefins production is favored by reducing the proportion of H_2 (decreasing the H_2/TCM molar ratio, Fig. 3(b)) while forming saturated hydrocarbons (CH_4 and C1 + paraffins) is disfavored. With less adsorbed-H, its 'diluting' effect on the Pd center surface also decreases, facilitating the interaction between nearby radicals adsorbed on adjacent centers to form C–C bonds, disfavoring the production of CH_4 . As the hydrogenation process is hindered because of the lowest proportion of available hydrogen, the formed olefins could be more easily desorbed from the reactive sites. Herein, the formation of olefins is promoted, whereas the formation of paraffins is inhibited. In addition, when reducing the H_2/TCM , the dechlorination ability of PdCl/CNF decreases evidently ($50\text{H}_2/\text{TCM}$: 98.5 %; $10\text{H}_2/\text{TCM}$: 92 %) (Fig. 3(d)) leading to an increase of selectivity to chloromethanes, while this is not remarkable in PdCl/CNT (dechlorination grade: $50\text{H}_2/\text{TCM}$: 98.5 %; $10\text{H}_2/\text{TCM}$: 97.5 %) (Fig. 3(b)). This confirms the stronger

dechlorination ability of PdCl/CNT.

When reducing the proportion of H₂ in the reaction using the PdCl-based catalysts (Fig. 3(a) and 4), a fast decrease in conversion is advised for PdCl/CNF. At the same time, for PdCl/CNT, only a slight deactivation is observed after a steady-state period under the stream. These results suggest stronger adsorption of TCM, intermediates, or both on the Pd active centers, inhibiting HDC reaction when reducing the proportion of H₂. PdCl/CNT, with smaller and well-distributed Pd NPs, could resist this effect since much more active centers are available for the reaction. Besides, its high stability at lower H₂ proportions (Fig. 3(a)) confirms again that small Pd NPs sizes and high electron-density hinder the poisoning of active centers and, consequently, promote stability.

In all the cases, the selectivity to saturated hydrocarbons (C1 + paraffins) is maximum at the beginning of the reaction (Figs. 2 and 4). After that, some slightly decreases are notified, whereas the selectivity to olefins somewhat increases. The active centres' hydrogenation ability may weaken when the reactants and formed intermediates are chemisorbed on the Pd centers until they saturate them. Once the surface has been saturated, the accessibility of reactants to active sites and surface properties of the catalyst may change, modifying the selectivity. In addition, if reactants remain adsorbed for a long time, they prevent H₂ activation favoring the C–C coupling against hydrogenolysis. The contribution of these phenomena is supported by the changes observed in the evolution of selectivity when reducing the H₂/TCM molar ratio (Fig. 4).

Fig. 4 shows a slighter olefins selectivity increase with time on stream when reducing H₂/TCM molar ratio, reaching a steady-state earlier for both catalysts, confirming that the higher electron density of the catalyst favors the formation of olefins with better stability. Thus, the H₂/TCM = 10 seems to be the optimum condition for TCM HDC with PdCl/CNT since high activity and high stable selectivity to olefins remain. In the case of PdCl/CNF, no significant increase of selectivity to olefins is observed when reducing the H₂/TCM ratio from 25 to 10 (Fig. 3(d), 4(e and f)), which could be ascribed to the loss of dechlorination ability caused by the strong deactivation, in agreement to the significant increase of selectivity to chloromethanes (Fig. 3(d)).

5. Conclusions

The new approach of using Pd-based catalyst supported on carbon nanotubes synthesized using PdCl₂ as Pd precursor (PdCl/CNT) to upgrade waste chloroform (TCM) for producing valuable light olefins employing hydrodechlorination (HDC) reaction shows competitive results. An outstanding catalytic activity (>90 %) with high and stable selectivity to light olefins (>80 %) is obtained when operating with an H₂/TCM molar ratio of 10. This selectivity to light olefins is much higher and more stable than that reported in some previous studies [9,10].

PdCl/CNT shows remarkable stability, even when operating at low space–time. Moreover, it shows the highest activity among the four catalysts tested and the highest selectivity to olefins. This has been ascribed to its smallest and well-distributed Pd nanoparticles (NPs), formed via the relatively high CNT surface area, the highest electron density of its Pd NPs, the strong Pd precursor-support interaction, and the low concentration of carboxylic acid groups.

Among the four studied catalysts (PdCl/CNT, PdCl-based catalyst supported on carbon nanofibers (CNF) (PdCl/CNF), Pd-based catalyst using Pd(NO₃)₂ as Pd precursor supported on CNT (PdN/CNT) and PdN/CNF), Pd NPs sizes increase following the order PdCl/CNT < PdCl/CNF ~ PdN/CNT < PdN/CNF, descending the electron density of Pd NPs in a similar order.

The electron density of the Pd NPs is a critical factor in the reaction that influences the selectivity and catalysts' stability. The electron density is determined by the carbon support and Pd precursor used since they define the final NPs sizes and the electron withdrawal-donation balance from the support.

The chloride precursor presents better catalytic behavior than the

nitrate one regardless of the support. Cl ions favor the donation of electrons from the support to the Pd NPs, playing an essential role in the electronic properties of the support. The donation of electrons is evident in PdCl/CNT since CNT provides delocalized π electrons, transforming the 4d-band of Pd. In PdCl/CNF, PdN/CNT, and PdN/CNF, the bigger Pd NPs compensate for this effect. The donation of electrons in PdN/CNT is not noticed, while in PdCl/CNF, Pd NPs show somewhat higher electron density despite their similar Pd NPs sizes. PdN/CNF, with the less suitable support and precursor and the biggest Pd NPs among the four tested catalysts, presents some Pdⁿ⁺ species. PdCl/CNT, with the highest electron density of Pd NPs among the four tested catalysts, shows an excellent stable activity, even when reducing the H₂ proportion. In addition, when employing a lower space–time, PdCl/CNT still shows high stability. On the contrary, the larger Pd NPs with much lower electron density in PdCl/CNF, PdN/CNT, and PdN/CNF contribute to the formation of PdC_x in the initial stage of the reaction, causing strong deactivation of the active sites.

The high selectivity to olefins of PdCl/CNT, obtained mainly as a consequence of the high electron density and small sizes of Pd NPs, is also favored when reducing the H₂ proportion.

The production of CH₄ is related to a lower electron density of Pd centers. The formation of PdC_x may also promote its production since the expansion of distance between the Pd atoms disfavors the formation of C–C bonds.

This work provides a promising catalyst, PdCl/CNT to efficiently upgrade the waste TCM into light olefins by HDC, and clearly explains the effects of catalyst surface nature in the Pd NPs electron density and sizes, and in the catalyst performance. In future studies, higher concentrations of TCM should be used to check the process's effectiveness. Also, a more in-depth study can be carried out regarding understanding the effect of different parameters such as morphology of Pd NPs in the catalyst properties and the catalytic performance.

Data availability

Data will be made available on request.

CRediT authorship contribution statement

Sichen Liu: Conceptualization, Investigation, Methodology, Formal analysis, Validation, Data curation, Writing – original draft, Writing – review & editing. **Carlos Fernandez-Ruiz:** Conceptualization, Investigation, Methodology, Formal analysis, Data curation. **Ana Iglesias-Juez:** Resources, Investigation, Methodology, Formal analysis, Validation, Data curation, Writing – original draft, Writing – review & editing, Supervision. **Maria Martin-Martinez:** Conceptualization, Investigation, Methodology, Validation, Data curation, Writing – review & editing, Funding acquisition, Supervision. **Jorge Bedia:** Conceptualization, Investigation, Methodology, Validation, Writing – review & editing, Supervision. **Carlo Marini:** Resources. **Giovanni Agostini:** Resources. **Juan José Rodriguez:** Writing – review & editing, Supervision. **Luisa María Gómez-Sainero:** Conceptualization, Investigation, Methodology, Formal analysis, Validation, Data curation, Writing – review & editing, Funding acquisition, Project administration, Supervision.

Declaration of Competing Interest

The authors declare the following financial interests/personal relationships which may be considered as potential competing interests: [Luisa Maria Gomez-Sainero reports financial support was provided by Spanish Ministry of Science, Innovation and Universities. Maria Martin-Martinez reports financial support was provided by Community of Madrid. Luisa Maria Gomez-Sainero reports financial support was provided by ALBA Synchrotron].

Data availability

Data will be made available on request.

Acknowledgements

The authors acknowledges FEDER/Ministerio de Ciencia, Innovación y Universidades – Agencia Estatal de Investigación (CTM2017-85498-R) and Comunidad de Madrid/UAM (SI1/PJ1/2019-00487) for financial support. The authors acknowledge to ALBA Synchrotron facility for beamtime at CLAES (experiment 2016021666-2). Maria Martin-Martinez acknowledges a postdoctoral grant (2017-T2/AMB-5668), from the Comunidad de Madrid “Atracción de Talento” programme. Sichen Liu acknowledges Ministerio de Ciencia e Innovación for his research grant (PRE2018-084424).

Appendix A. Supplementary data

Supplementary data to this article can be found online at <https://doi.org/10.1016/j.jcis.2023.05.169>.

References

- [1] M. Martin-Martinez, L.M. Gómez-Sainero, M.A. Alvarez-Montero, J. Bedia, J. J. Rodríguez, Comparison of different precious metals in activated carbon-supported catalysts for the gas-phase hydrodechlorination of chloromethanes, *Appl. Catal. B: Environ.* 132–133 (2013) 256–265, <https://doi.org/10.1016/j.apcatb.2012.11.041>.
- [2] B. Huang, C. Lei, C. Wei, G. Zeng, Chlorinated volatile organic compounds (Cl-VOCs) in environment—Sources, potential human health impacts, and current remediation technologies, *Environ. Int.* 71 (2014) 118–138, <https://doi.org/10.1016/j.envint.2014.06.013>.
- [3] P.M. Schlosser, A.S. Bale, C.F. Gibbons, A. Wilkins, G.S. Cooper, Human health effects of dichloromethane: Key findings and scientific issues, *Environ. Health Perspect.* 123 (2015) 114–119, <https://doi.org/10.1289/ehp.1308030>.
- [4] S. Liu, J.A. Otero, M. Martin-Martinez, D. Rodríguez-Franco, J.J. Rodríguez, L. M. Gómez-Sainero, Understanding hydrodechlorination of chloromethanes. Past and future of the technology, *Catalysts* 10 (2020) 1462, <https://doi.org/10.3390/catal10121462>.
- [5] M. Martin-Martinez, A. Álvarez-Montero, L.M. Gómez-Sainero, R.T. Baker, J. Palomar, S. Omar, S. Eser, J.J. Rodríguez, Deactivation behavior of Pd/C and Pt/C catalysts in the gas-phase hydrodechlorination of chloromethanes: Structure–reactivity relationship, *Appl. Catal. B Environ.* 162 (2015) 532–543, <https://doi.org/10.1016/j.apcatb.2014.07.017>.
- [6] L.M. Gómez-Sainero, J. Palomar, S. Omar, C. Fernández, J. Bedia, A. Álvarez-Montero, J.J. Rodríguez, Valorization of chloromethanes by hydrodechlorination with metallic catalysts, *Catal. Today* 310 (2018) 75–85, <https://doi.org/10.1016/j.cattod.2017.05.006>.
- [7] J.C. Velazquez, S. Leekumjorn, Q.X. Nguyen, Y.-L. Fang, K.N. Heck, G.D. Hopkins, M. Reinhard, M.S. Wong, Chloroform hydrodechlorination behavior of alumina-supported Pd and PdAu catalysts, *AIChE J.* 59 (12) (2013) 4474–4482, <https://doi.org/10.1002/aic.14250>.
- [8] A.N. Ardila A, J. Reyes, E. Arriola, J.A. Hernández, G.A. Fuentes, Liquid-phase chloroform hydrodechlorination catalyzed by Pd/TiO₂-Na, *Appl. Catal. A: Gen.* 497 (2015) 211–215, <https://doi.org/10.1016/j.apcata.2015.02.045>.
- [9] C. Fernandez-Ruiz, J. Bedia, S. Andreoli, S. Eser, J.J. Rodríguez, L.M. Gómez-Sainero, Selectivity to olefins in the hydrodechlorination of chloroform with activated carbon-supported palladium catalysts, *Ind. Eng. Chem. Res.* 58 (2019) 20592–20600, <https://doi.org/10.1021/acs.iecr.9b04262>.
- [10] C. Fernandez-Ruiz, J. Bedia, J.M. Grau, A.C. Romero, D. Rodríguez, J.J. Rodríguez, L.M. Gómez-Sainero, Promoting light hydrocarbons yield by catalytic hydrodechlorination of residual chloromethanes using palladium supported on zeolite catalysts, *Catalysts* 10 (2020) 199, <https://doi.org/10.3390/catal10020199>.
- [11] Y. Wei, D. Zhang, Z. Liu, B.-L. Su, Methyl halide to olefins and gasoline over zeolites and SAPO catalysts: A new route of MTO and MTG, *Chin. J. Catal.* 33 (2012) 11–21, [https://doi.org/10.1016/S1872-2067\(10\)60303-8](https://doi.org/10.1016/S1872-2067(10)60303-8).
- [12] L.-T. Kong, B.-X. Shen, J.-G. Zhao, J.-C. Liu, Comparative study on the chloromethane to olefins reaction over SAPO-34 and HZSM-22, *Ind. Eng. Chem. Res.* 53 (2014) 16324–16331, <https://doi.org/10.1021/ie5028155>.
- [13] M. Gamero, A.T. Aguayo, A. Ateka, P. Pérez-Urriarte, A.G. Gayubo, J. Bilbao, Role of shape selectivity and catalyst acidity in the transformation of chloromethane into light olefins, *Ind. Eng. Chem. Res.* 54 (2015) 7822–7832, <https://doi.org/10.1021/acs.iecr.5b01745>.
- [14] L.-T. Kong, B.-X. Shen, Z. Jiang, J.-G. Zhao, J.-C. Liu, Synthesis of SAPO-34 with the presence of additives and their catalytic performance in the transformation of chloromethane to olefins, *React. Kinet. Mech. Catal.* 114 (2015) 697–710, <https://doi.org/10.1007/s11144-014-0812-1>.
- [15] L.M. Kartashov, V.N. Rozanov, Y.A. Treger, M.R. Flid, T.L. Kalyuzhnaya, D. V. Tkach, Processing the wastes from the production of methyl chloride in the synthesis of olefins from natural gas, *Catal. Ind.* 2 (2010) 230–238, <https://doi.org/10.1134/S20770050410030050>.
- [16] M.H. Nilsen, S. Svelle, S. Aravinthan, U. Olsbye, The conversion of chloromethane to light olefins over SAPO-34: The influence of dichloromethane addition, *Appl. Catal. A: Gen.* 367 (2009) 23–31, <https://doi.org/10.1016/j.apcata.2009.07.047>.
- [17] M. Martin-Martinez, J.J. Rodríguez, R.T. Baker, L.M. Gómez-Sainero, Deactivation and regeneration of activated carbon-supported Rh and Ru catalysts in the hydrodechlorination of chloromethanes into light olefins, *Chem. Eng. J.* 397 (2020), 125479, <https://doi.org/10.1016/j.cej.2020.125479>.
- [18] P. Serp, M. Corrias, P. Kalck, Carbon nanotubes and nanofibers in catalysis, *Appl. Catal. A: Gen.* 253 (2003) 337–358, [https://doi.org/10.1016/S0926-860X\(03\)00549-0](https://doi.org/10.1016/S0926-860X(03)00549-0).
- [19] P. Serp, E. Castillejos, Catalysis in carbon nanotubes, *ChemCatChem* 2 (2010) 41–47, <https://doi.org/10.1002/cctc.200900283>.
- [20] K.P. De Jong, J.W. Geus, Carbon nanofibers: Catalytic synthesis and applications, *Catal. Rev.—Sci. Eng.* 42(4) (2000) 481–510, [10.1081/CR-100101954](https://doi.org/10.1081/CR-100101954).
- [21] Y. Yan, J. Miao, Z. Yang, F.-X. Xiao, H.B. Yang, B. Liu, Y. Yang, Carbon nanotube catalysts: recent advances in synthesis, characterization and applications, *Chem. Soc. Rev.* 44 (2015) 3295–3346, <https://doi.org/10.1039/c4cs00492b>.
- [22] C. Amorim, G. Yuan, P.M. Patterson, M.A. Keane, Catalytic hydrodechlorination over Pd supported on amorphous and structured carbon, *J. Catal.* 234 (2005) 268–281, <https://doi.org/10.1016/j.jcat.2005.06.019>.
- [23] R.F. Bueres, E. Asedegbega-Nieto, E. Díaz, S. Ordóñez, F.V. Díez, Preparation of carbon nanofibres supported palladium catalysts for hydrodechlorination reactions, *Catal. Commun.* 9 (2008) 2080–2084, <https://doi.org/10.1016/j.catcom.2008.04.005>.
- [24] C.D. Wagner, L.E. Davis, M.V. Zeller, J.A. Taylor, R.H. Raymond, L.H. Gale, Empirical atomic sensitivity factors for quantitative analysis by electron spectroscopy for chemical analysis, *Surf. Interface Anal.* 3 (1981) 211–225, <https://doi.org/10.1002/sia.740030506>.
- [25] B. Ravel, M. Newville, ATHENA, ARTEMIS, HEPHAESTUS: data analysis for X-ray absorption spectroscopy using IFEFFIT, *J. Synchrotron Rad.* 12 (2005) 537–541, <https://doi.org/10.1107/S0909049505012719>.
- [26] Z.M. de Pedro, L.M. Gómez-Sainero, E. Gonzalez-Serrano, J.J. Rodríguez, Gas-phase hydrodechlorination of dichloromethane at low concentrations with palladium/carbon catalysts, *Ind. Eng. Chem. Res.* 45 (2006) 7760–7766, <https://doi.org/10.1021/ie060621m>.
- [27] K.S.W. Sing, Reporting physisorption data for gas/solid systems with special reference to the determination of surface area and porosity, *Pure & Appl. Chem.* 57 (4) (1985) 603–619, <https://doi.org/10.1351/pac198557040603>.
- [28] J.L. Figueiredo, M.F.R. Pereira, M.M.A. Freitas, J.J.M. Órfa, Modification of the surface chemistry of activated carbons, *Carbon* 37 (1999) 1379–1389, [https://doi.org/10.1016/S0008-6223\(98\)00333-9](https://doi.org/10.1016/S0008-6223(98)00333-9).
- [29] M. Martin-Martinez, M.F.F. Barreiro, A.M.T. Silva, J.L. Figueiredo, J.L. Faria, H. T. Gomes, Lignin-based activated carbons as metal-free catalysts for the oxidative degradation of 4-nitrophenol in aqueous solution, *Appl. Catal. B: Environ.* 219 (2017) 372–378, <https://doi.org/10.1016/j.apcatb.2017.07.065>.
- [30] M. Göckeler, C.M. Berger, M. Purcel, R. Bergstäßer, A.-P. Schinkel, M. Muhler, Surface reactions during temperature-programmed desorption and reduction experiments with oxygen-functionalized carbon blacks, *Appl. Surf. Sci.* 561 (2021), 150044, <https://doi.org/10.1016/j.apsusc.2021.150044>.
- [31] O.V. Netskina, O.V. Komova, E.S. Tayban, G.V. Oderova, S.A. Mukha, G. G. Kuvshinov, V.I. Simagina, The influence of acid treatment of carbon nanofibers on the activity of palladium catalysts in the liquid-phase hydrodechlorination of dichlorobenzene, *Appl. Catal. A: Gen.* 467 (2013) 386–393, <https://doi.org/10.1016/j.apcata.2013.07.046>.
- [32] Z.Q. Li, C.J. Lu, Z.P. Xia, Y. Zhou, Z. Luo, X-ray diffraction patterns of graphite and carbon nanotube, *Carbon* 45 (2007) 1686–1695, <https://doi.org/10.1016/j.carbon.2007.03.038>.
- [33] W. Chen, X. Pan, M.-G. Willinger, D.S. Su, X. Bao, Facile autoreduction of iron oxide/carbon nanotube encapsulates, *J. Am. Chem. Soc.* 128 (2006) 3136–3137, <https://doi.org/10.1021/ja0567211>.
- [34] J.C. Espinosa, R.C. Contreras, S. Navalón, C. Rivera-Cárcamo, M. Álvaro, B. F. Machado, P. Serp, H. García, Influence of carbon supports on palladium nanoparticle activity toward hydrodeoxygenation and aerobic oxidation in biomass transformations, *Eur. J. Inorg. Chem.* (2019) 1979–1987, <https://doi.org/10.1002/ejic.201900190>.
- [35] L.M. Gómez-Sainero, J.M. Grau, A. Arcaya, X.L. Seoane, Carbon-supported palladium catalysts for liquid-phase hydrodechlorination of carbon tetrachloride to chloroform, *Stud. Surf. Sci. Catal.* 130 (2000) 2009–2014, [https://doi.org/10.1016/S0167-2991\(00\)80763-6](https://doi.org/10.1016/S0167-2991(00)80763-6).
- [36] J.-P. Tessonnier, O. Ersen, G. Weinberg, C. Pham-Huu, D.S. Su, R. Schlögl, Selective deposition of metal nanoparticles inside or outside multi-walled carbon nanotubes, *ACS Nano* 3 (8) (2009) 2081–2089, <https://doi.org/10.1021/nn900647q>.
- [37] A. Iglesias-Juez, A. Kubacka, M. Fernandez-García, M.D. Michiel, M.A. Newton, Nanoparticulate Pd supported catalysts: Size-dependent formation of Pd(I)/Pd(0) and their role in CO elimination, *J. Am. Chem. Soc.* 133 (2011) 4484–4489, <https://doi.org/10.1021/ja110320y>.
- [38] D. Bazin, J.J. Rehr, Limits and advantages of X-ray absorption near edge structure for nanometer scale metallic clusters, *J. Phys. Chem. B* 107 (2003) 12398–12402, <https://doi.org/10.1021/jp0223051>.
- [39] A. Jenty, Estimation of mean size and shape of small metal particles by EXAFS, *Phys. Chem. Chem. Phys.* 1 (1999) 4059–4063, <https://doi.org/10.1039/A904654B>.

- [40] M. Altarelli, D.L. Dexter, H.M. Nussenzveig, D.Y. Smith, Superconvergence and sum rules for the optical constants, *Phys. Rev. B* 6 (1972) 4502–4509, <https://doi.org/10.1103/PhysRevB.6.4502>.
- [41] P. Kizler, X-ray-absorption near-edge structure spectra for bulk materials: Multiple-scattering analysis versus a phenomenological approach, *Phys. Rev. B* 46 (1992) 10540–10546, <https://doi.org/10.1103/PhysRevB.46.10540>.
- [42] R. Lässer, G.L. Powell, Solubility of H, D, and T in Pd at low concentrations, *Phys. Rev. B* 34 (1986) 578–586, <https://doi.org/10.1103/PhysRevB.34.578>.
- [43] S. Liu, M. Martín-Martínez, M.A. Álvarez-Montero, A. Arevalo-Bastante, J. J. Rodríguez, L.M. Gómez-Sainero, Recycling of gas phase residual dichloromethane by hydrodechlorination: regeneration of deactivated Pd/C catalysts, *Catalysts* 9 (2019) 733, <https://doi.org/10.3390/catal9090733>.
- [44] T. Gong, L. Qin, W. Zhang, H. Wan, J. Lu, H. Feng, Activated carbon supported palladium nanoparticle catalysts synthesized by atomic layer deposition: Genesis and evolution of nanoparticles and tuning the particle size, *J. Phys. Chem. C* 119 (2015) 11544–11556, <https://doi.org/10.1021/jp5130102>.
- [45] I.C. Gerber, P. Serp, A theory/experience description of support effects in carbon-supported catalysts, *Chem. Rev.* 120 (2020) 1250–1349, <https://doi.org/10.1021/acs.chemrev.9b00209>.
- [46] H. Lu, B. Xu, X. Wang, Z. Hu, Y. Fan, The influence of Pd particles distribution position on Pd/CNTs catalyst for acetylene selective hydrogenation, *Catal. Lett.* 144 (2014) 2198–2203, <https://doi.org/10.1007/s10562-014-1388-0>.
- [47] J. Wang, S.-M. Lu, J. Li, C. Li, A remarkable difference in CO₂ hydrogenation to methanol on Pd nanoparticles supported inside and outside of carbon nanotubes, *Chem. Commun.* 51 (2015) 17615–17618, <https://doi.org/10.1039/C5CC07079A>.
- [48] X. Blase, L.X. Benedict, E.L. Shirley, S.G. Louie, Hybridization effects and metallicity in small radius carbon nanotubes, *Phys. Rev. Lett.* 72 (1994) 1878–1881, <https://doi.org/10.1103/PhysRevLett.72.1878>.
- [49] D. Ugarte, A. Châtelain, W.A. de Heer, Nanocapillarity and chemistry in carbon nanotubes, *Science* 274 (1996) 1897–1899, <https://doi.org/10.1126/science.274.5294.1897>.
- [50] R.G. Rao, R. Blume, T.W. Hansen, E. Fuentes, K. Dreyer, S. Moldovan, O. Ersen, D. D. Hibbitts, Y.J. Chabal, R. Schlögl, J.-P. Tessonnier, Interfacial charge distributions in carbon-supported palladium catalysts, *Nat. Commun.* 8 (2017) 340, <https://doi.org/10.1038/s41467-017-00421-x>.
- [51] A. Kubacka, A. Martínez-Arias, M. Fernández-García, M.D. Michiel, M.A. Newton, Multitechnique analysis of supported Pd particles upon dynamic, cycling CO/NO conditions: Size-dependence of the structure–activity relationship, *J. Catal.* 270 (2010) 275–284, <https://doi.org/10.1016/j.jcat.2010.01.008>.
- [52] L. Ebersson, Electron transfer reactions in organic chemistry. II.* An analysis of alkyl halide reduction by electron transfer reagents on the basis of the marcus theory, *Acta Chem. Scand. B* 36 (1982) 533–543, <https://doi.org/10.3891/acta.chem.scand.36b-0533>.
- [53] M. Elsner, S.B. Haderlein, T. Kellerhals, S. Luzzi, L. Zwank, W. Angst, R. P. Schwarzenbach, Mechanisms and products of surface-mediated reductive dehalogenation of carbon tetrachloride by Fe(II) on goethite, *Environ. Sci. Technol.* 38 (2004) 2058–2066, <https://doi.org/10.1021/es034741m>.
- [54] S. Omar, J. Palomar, L.M. Gómez-Sainero, M.A. Álvarez-Montero, M. Martín-Martínez, J.J. Rodríguez, Density functional theory analysis of dichloromethane and hydrogen interaction with Pd clusters: First step to simulate catalytic hydrodechlorination, *J. Phys. Chem. C* 115 (2011) 14180–14192, <https://doi.org/10.1021/jp200329j>.
- [55] L. Xu, S. Bhandari, J. Chen, J. Glasgow, M. Mavrikakis, Chloroform hydrodechlorination on palladium surfaces: A comparative DFT study on Pd(111), Pd(100), and Pd(211), *Top. Catal.* 63 (2020) 762–776, <https://doi.org/10.1007/s11244-019-01218-6>.
- [56] A. Arevalo-Bastante, S. Omar, J. Palomar, M.A. Álvarez-Montero, J. Bedia, J. J. Rodríguez, L.M. Gómez-Sainero, Design of hydrodechlorination catalysts on the basis of chloromethanes-metallic active sites interactions, *Chem. Eng. J.* 446 (2022), 136893, <https://doi.org/10.1016/j.cej.2022.136893>.
- [57] B. Yang, R. Burch, C. Hardacre, P. Hu, P. Hughes, Importance of surface carbide formation on the activity and selectivity of Pd surfaces in the selective hydrogenation of acetylene, *Surf. Sci.* 646 (2016) 45–49, <https://doi.org/10.1016/j.susc.2015.07.015>.
- [58] J. Osswald, K. Kovnir, M. Armbrüster, R. Giedigkeit, R.E. Jentoft, U. Wild, Y. Grin, R. Schlögl, Palladium-gallium intermetallic compounds for the selective hydrogenation of acetylene: Part II: Surface characterization and catalytic performance, *J. Catal.* 258 (2008) 219–227, <https://doi.org/10.1016/j.jcat.2008.06.014>.